文章编号：1001-9014(2021)02-0166-06

DOI:10.11972/j.issn.1001-9014.2021.02.005

The heterostructure $NaGdF_4$:Yb,Er nanorods loaded on metal-organic frameworks for tuning upconversion photoluminescence

LIU Yi, JIAO Ji-Qing*, LYU Bai-Ze, WANG Jiu-Xing

(College of Materials Science and Engineering, National Center of International Joint Research for Hybrid Materials Technology, National Base of International Sci. & Tech. Cooperation, Qingdao University, Qingdao 266071, China)

Abstract: Multi-component heterostructure nanocomposites can not only inherit the original properties of each component, but also induce new chemical and electronic properties through the interaction between the components. The heterostructure zeolitic imidazolate framework/$NaGdF_4$: Yb, Er (ZIF-67/$NaGdF_4$: Yb, Er) was prepared by a stepwise synthesis strategy. And it avoided agglomeration and quenching of upconversion (UC) nanoparticles, and displayed better stability. In the heterostructure nanocomposites, ZIF-67 is employed as an energy transmission platform under 980 nm excitation. Compared to pure $NaGdF_4$: Yb, Er nanorods, the UC photoluminescence of heterostructure ZIF-67/$NaGdF_4$: Yb, Er is tuned from green to red owing to the synergistic effect of each component.

Key words: heterostructure, controllable synthesis, nanocomposite, luminescence, upconversion

PACS: 42

异质结构—$NaGdF_4$:Yb,Er纳米棒负载在金属有机框架上以调节上转换光致发光

刘 毅, 焦吉庆*, 吕柏泽, 王久兴

(青岛大学 材料科学与工程学院 国家杂化材料技术国际联合研究中心 国际科学技术合作国家基地,山东 青岛 266071)

摘要:多组分异质结构纳米复合材料不仅可以继承每个组分原有的性能,而且还可以通过组分之间的相互作用诱导出新的化学、电子性能。通过逐步合成法制备的异质结构的金属有机框架/$NaGdF_4$:Yb,Er(ZIF-67/$NaGdF_4$:Yb,Er)复合材料避免了上转换(UC)纳米粒子的团聚和淬灭,并显示了更好的稳定性。在异质结构纳米复合材料中,ZIF-67被用作980 nm激发下的能量传输平台。与$NaGdF_4$:Yb,Er纳米棒相比,由于各组分间的协同作用,异质结构ZIF-67/$NaGdF_4$:Yb,Er的UC光致发光从绿色调为红色。

关 键 词:异质结构;可控合成;纳米复合材料;光致发光;上转换

中图分类号:O439 **文献标识码**:A

Introduction

Multi-component heterostructure nanocomposites, which composed of two or more nanomaterials, can inherit the unique properties and overcome the limitation of single component [1-2]. At the same time, the multi-component heterostructure can endow many new properties, such as magnetism, light, electricity and etc. [3-6]. Photon upconversion (UC) has the ability to converting near infrared (NIR) photons into visible or ultraviolet (UV) radiation, it is a unique imaging technique that utilizes low photon energy [7-8]. The UC nanomaterials are composed of matrix doped with rare earth ions used as sensitizer and activators. And modification of luminescence

Received date: 2020-05-29, **revised date**: 2020-12-28 **收稿日期**:2020-05-29,**修回日期**:2020-12-28

Foundation items: Supported by National Natural Science Foundation of China (51403114, 51703104), Science and Technology Innovation Program of Universities of Shandong Province (2020KJA012), Natural Science Foundation of Shandong Province (BS2014CL025, ZR2017BEM035), China Postdoctoral Science Foundation (2014M56053, 2017M612198), Postdoctoral Innovation Fund of Shandong Province (201402015), Program for Introducing Talents of Discipline to Universities ("111"plan)

Biography: LIU Yi (1992-), male, Qingdao, China, master. Research area involves Upconverting nanoparticles excited by near infrared light
E-mail: 1356011573@qq.com

* **Corresponding author**: E-mail: jiaojiqing101@163.com

can be achieved by changing the type of rare earth ions. Owing to the low photon energy, high rare-earth ion solubility and good thermal stability, the rare-earth fluorides ($NaREF_4$) are the most effective matrix. $NaGdF_4$ is as candidate own to lower vibrational phonon energy and matching lattice with doped ions [9-10]. Besides, the hexagonal phase $NaGdF_4$ can improve the luminous efficiency of UC, and Gd^{3+} has a large energy level interval, it can also pass sensitization ion (Yb^{3+}) and activation ion (Er^{3+}, Tm^{3+} and Ho^{3+}) achieves high-efficiency UC luminescence. Er^{3+} has fluorescence response of blue, green and red light, and the emission could be adjusted by tuning structure. Therefore, $NaGdF_4$: Yb, Er has the advantages of low excitation energy, high luminous efficiency and good thermal stability, so it has potential application prospects in biological imaging, drug delivery, tumor treatment, display equipment, solar energy conversion, etc. [11-12]. However, $NaGdF_4$: Yb, Er has a tendency to aggregate and quench, which greatly reduces its photoluminescence (PL) performance, and the oil phase system limits its application. Meanwhile, realizing the tuning of light is expected to broaden the application range of $NaGdF_4$: Yb, Er. In order to make up for its shortcomings, many strategies had been reported, such as forming core-shell structure, tuning size or morphology and constructing the composites[13-15]. Among many methods, construction heterostructure by compounding with other materials can not only improve the stability and compatibility of $NaGdF_4$: Yb, Er, but also tuning optical properties.

Metal-organic frameworks (MOFs) are a class of carrier materials with unprecedented chemical and structural tunability. Their synthetic controllability and structural design properties make MOFs as ideal platforms for identifying design features for advanced functional materials[16]. Meanwhile, MOFs are considered as promising energy transmission (ET) platform to achieve collaborative molecular level functions and promote efficient energy transfer due to the highly accessible and spatially discrete linkers[17]. Li et al. integrated UC nanoparticles and MOF to construct a composite photocatalyst that has adjustable photocatalytic activity[18]. Chen et al. prepared core-shell UC nanoparticle@MOF nanoprobes for luminescent/magnetic dual-mode targeted imaging[13]. In our work, MIL-101/$NaGdF_4$: Yb, Er were prepared by the two-step method, the photocatalyst displayed higher photocurrent and better degradation ability for Rhodamine B owing to synergistic effect[14]. Those works make full use of the adsorption and good bio-compatibility of MOFs. Zeolitic imidazolate frameworks (ZIFs) is a nitrogen-containing MOFs material obtained by compounding an imidazole or purine organic ligand with a transition metal ion. In particular, ZIF-67 is a regular dodecahedral structure material containing Co^{2+}, it has the advantages of high stability, high porosity, and large specific surface area[19]. The multiple energy levels contained in Co^{2+} can meet the energy exchange requirements with rare earth ions[20]. Therefore, construction heterostructure containing ZIF-67 is an effective strategy to broaden the application prospect of $NaGdF_4$: Yb, Er while achieving light tuning.

Here in, we have prepared multi-component heterostructure ZIF-67/$NaGdF_4$: Yb, Er by a stepwise synthesis method. The $NaGdF_4$: Yb, Er nanorods were loaded on the surface of ZIF-67, which was used as a carrier. The heterostructure ZIF-67/$NaGdF_4$: Yb, Er, which avoided agglomeration and quench of UC nanoparticles, display better stability. Meanwhile, the composites improved the compatibility of alcohol, so that it broke through the constraints of oil phase systems. ZIF-67 is also used as an ET platform to achieve UC PL tuning of $NaGdF_4$: Yb, Er nanorods by energy transition. Compared with $NaGdF_4$: Yb, Er nanorods under 980 nm laser excitation, the PL performance of heterostructure ZIF-67/$NaGdF_4$: Yb, Er has converted from green light to red light that owing to the synergistic effect between individual components. The incorporation of ZIF-67 alter the PL performance of $NaGdF_4$: Yb, Er nanorods and lead to a heterostructure with good stability, which broadens the application and promotes the progress of key technologies in the field of photon UC nanomaterials.

1 Experiments

1.1 Synthesis of $NaGdF_4$: Yb, Er upconversion nanoparticles

In a typical preparation, 1.2 g NaOH was dissolved in 2 ml deionized water and ultrasonically dispersed. After the heat released, the solution was heating and stirring in a 50 ℃ water bath. Next, 8 ml alcohol and 20 ml oleic acid were added to the above solution under stirring 20 min to be a transparent solution. 1 mmol of $Ln(NO_3)_3 \cdot 6H_2O$ (Ln: 78% Gd; 20% Yb; 2% Er) aqueous solution were added under vigorous stirring. Then, 0.8 g PVP dissolved in 3 ml of ethanol and add to above solution. Subsequently, 8 ml of NaF aqueous solution (1 mol/L) was added dropwise to the solution. Keep stirring to give it had a good dispersion to form a translucent colloidal solution. Finally, the mixed solution was transferred into reaction kettle and heated at 180 ℃ for 18 h. After reaction was completed, the system was cooled to room temperature naturally. The prepared samples were separated and washed used deionized water and ethanol by centrifugation to remove oleic acid and other remnants, and was stored in cyclohexane solvent.

1.2 Synthesis of ZIF-67

0.2911g of $Co(NO_3)_2 \cdot 6H_2O$ and 0.3284 g of 2-methylimidazole was dissolved in 25 ml of methanol and ultrasound for 10 min, respectively. Then the dissolved 2-methylimidazole solution was added dropwise to the $Co(NO_3)_2 \cdot 6H_2O$ solution, and stirred at room temperature for 3 h. Finally, the samples were separated to remove other remnants and stored in methanol.

1.3 Synthesis of the heterostructure ZIF-67/$NaGdF_4$:Yb,Er

Briefly, the prepared $NaGdF_4$: Yb, Er nanorods and ZIF-67 were mixed together. And then some PVP was added as dispersant, the mixture were stirred at 50 ℃ for 24 h. Finally, the samples were separated and washed to

remove other remnants and stored in methanol.

2 Results and discussions

As showed in Fig. 1, firstly, the $NaGdF_4$: Yb, Er nanorods was prepared at 180℃ and react for 18 h by hydrothermal treatment, which experience three-stage is nucleation, growth and regrowth during the reaction. And then, $NaGdF_4$: Yb, Er nanorods were added into ZIF-67, which prepared at room temperature for 3 h. Meanwhile, some PVP was added in the mixture as dispersant to prevent $NaGdF_4$: Yb, Er nanorods from aggregation. Finally, this mixture was string at 50℃ for 24 h to obtained heterostructure ZIF-67/$NaGdF_4$: Yb, Er. The detailed information of experiment could be found from Supplementary material

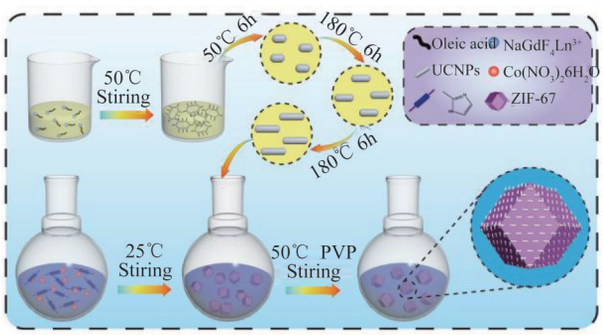

Fig. 1 Illustration for the preparation of heterostructure ZIF-67/$NaGdF_4$: Yb, Er
图1 异质结构ZIF-67/$NaGdF_4$:Yb,Er的制备流程图

The morphology of samples are characterized via transmission electron microscopy (TEM). As shown in Fig. 2(a), the length of prepared $NaGdF_4$: Yb, Er nanorods are around 50 nm. And the corresponding high-resolution transmission electron microscopy (HRTEM) image (inset of Fig. 2(a)) reveals clear lattice fringes with an inter-planar spacing of 0.49 nm, which is ascribed to the (101) plane of β-$NaGdF_4$: Yb, Er. The result was consistent with hexagonal phase (PDF: 27-0699), and determined by X-ray diffraction (XRD) (Fig. 3(a)). The size of ZIF-67 was approximately 500 nm, and it exhibited a typical and regular dodecahedron (Fig. 2(b)). As shown in Fig. 2(c-d), the $NaGdF_4$: Yb, Er nanorods are uniformly loaded on the surface of ZIF-67, and it was confirmed to be $NaGdF_4$: Yb, Er nanorods by HRTEM (Inset of Fig. 2(d)). Furthermore, as shown in energy dispersive X-ray spectroscopy (EDS), the Co element (from ZIF-67) was mainly distributed in the inside, and the F, Gd, Yb and Er elements (from $NaGdF_4$: Yb, Er nanorods) were homogeneously distributed throughout the heterostructure (Fig. 2(e)). And the Fourier transform infrared (FT-IR) spectra (Fig. 3(b)) evidenced the formation of heterostructure in ZIF-67/$NaGdF_4$: Yb, Er, this is consistent with the TEM and EDS results. From above analysis, the heterostructure ZIF-67/$NaGdF_4$: Yb, Er was prepared successfully.

The UC PL properties and conversion mechanism of heterostructure ZIF-67/$NaGdF_4$: Yb, Er were measured.

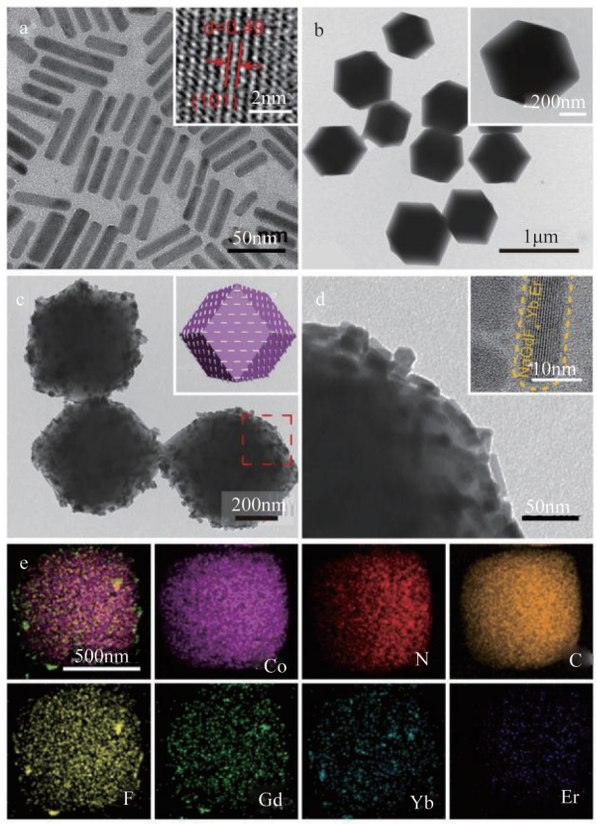

Fig. 2 The morphological characterization of heterostructure ZIF-67/$NaGdF_4$: Yb, Er (a) TEM image of $NaGdF_4$: Yb, Er nanorods, the inset is HRTEM image taken from (a), (b) TEM image of ZIF-67, (c) TEM image of heterostructure ZIF-67/$NaGdF_4$: Yb, Er, the inset is 3D model of (c), (d) The partial enlargement of (c), the inset is HRTEM image taken from (c), (e) EDS elemental mapping of heterostructure ZIF-67/$NaGdF_4$: Yb, Er.
图2 异质结构ZIF-67/$NaGdF_4$:Yb,Er的形貌表征(a)$NaGdF_4$:Yb,Er纳米棒的透射电镜图,插图是其高分辨透射电镜图,(b)ZIF-67的透射电镜图;(c)异质结构ZIF-67/$NaGdF_4$:Yb,Er的透射电镜图和它的3D模型(插图),(d)异质结构ZIF-67/$NaGdF_4$:Yb,Er的局部放大投射电镜图和高分辨透射电镜图(插图),(e)ZIF-67/$NaGdF_4$:Yb,Er的元素分布

As shown in Fig. 4(a), compared with PL performance of $NaGdF_4$: Yb, Er nanorods under 980 nm laser excitation, the green light (541 nm) of heterostructure ZIF-67/$NaGdF_4$: Yb, Er was drastically reduced and the red light (658 nm) was enhanced largely. And compared with ZIF-67, the red light has a significant enhanced, indicates that the PL tuning was attributed to the formation of the heterostructure. The absorption of heterostructure composites were further explored via UV-vis spectroscopy (Fig. 4(b)). The heterostructure ZIF-67/$NaGdF_4$: Yb, Er exhibited a broader absorption range and higher absorption strength compared with each component. Meanwhile, a new absorption peak appeared in the green region (510 nm-630 nm) compared with $NaGdF_4$: Yb, Er nanorods, which was contributed by ZIF-67. As shown in Fig. 4(c), the heterostructure ZIF-67/$NaGdF_4$: Yb, Er emitted red light (658 nm) under 541 nm laser excitation owing to the synergistic effect between ZIF-67 and

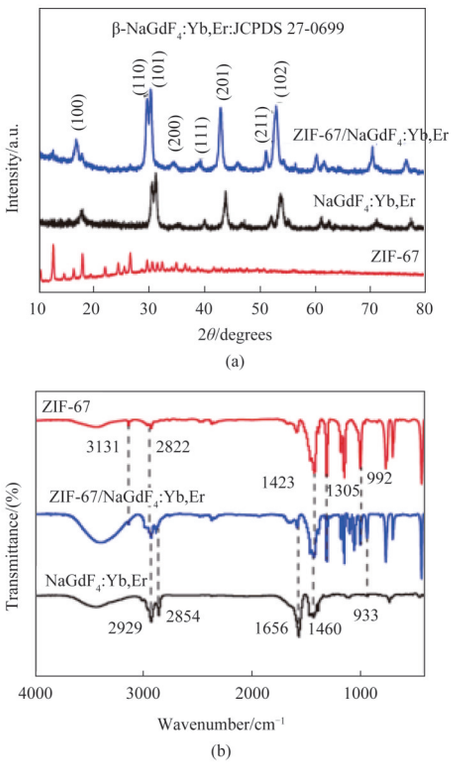

Fig. 3　The XRD and FT-IR spectra of heterostructure ZIF-67/$NaGdF_4$: Yb, Er

图3　异质结构ZIF-67/$NaGdF_4$: Yb, Er的X射线衍射和红外谱

$NaGdF_4$: Yb, Er nanorods. The photon energy of 541 nm was absorbed by ZIF-67 and emitted as red light (635 nm) through energy level transition, then transited to the energy level of Er^{3+} through photon relaxation, finally appeared as 658 nm emission of Er^{3+}. This mechanism will be further discussed in Fig. 6. Benefiting from the construction of heterostructure, this ZIF-67/$NaGdF_4$: Yb, Er achieved PL tuning and improved intensity of luminescence, which broadens its scope of application.

More interestingly, it found that the intensity of PL was related to the ratio of $NaGdF_4$: Yb, Er and ZIF-67 as shown in Fig. 4d. With the amount of $NaGdF_4$: Yb, Er increased, the intensity of red light (658 nm) enhanced linearly and remains unchanged after reaching the maximum. This is due to saturation of $NaGdF_4$: Yb, Er loading on ZIF-67, which could be further verified by TEM (Fig. 5). And the aggregated $NaGdF_4$: Yb, Er nanorods could be found when the amount of $NaGdF_4$: Yb, Er was increased after saturation (30%). Therefore, the heterostructure ZIF-67/$NaGdF_4$: Yb, Er not only tune PL emission, but also improved stability.

As can be seen from Fig. 4, the emission peak of the heterostructure ZIF-67/$NaGdF_4$: Yb, Er appeared at 658 nm is corresponding to the energy level transition of Er^{3+}. Without ZIF-67, the energy transfer process of $NaGdF_4$: Yb, Er is as follows[15]: the electrons in the $^2F_{7/2}$ ground state of Yb^{3+} are excited to the $^2F_{5/2}$ excited states after absorbing the 980 nm excitation. And then the energy is transferred to $^2I_{11/2}$, $^4F_{9/2}$, and $^4F_{7/2}$ level of Er^{3+} by radiation [21]. Subsequently, the energy transferred to the

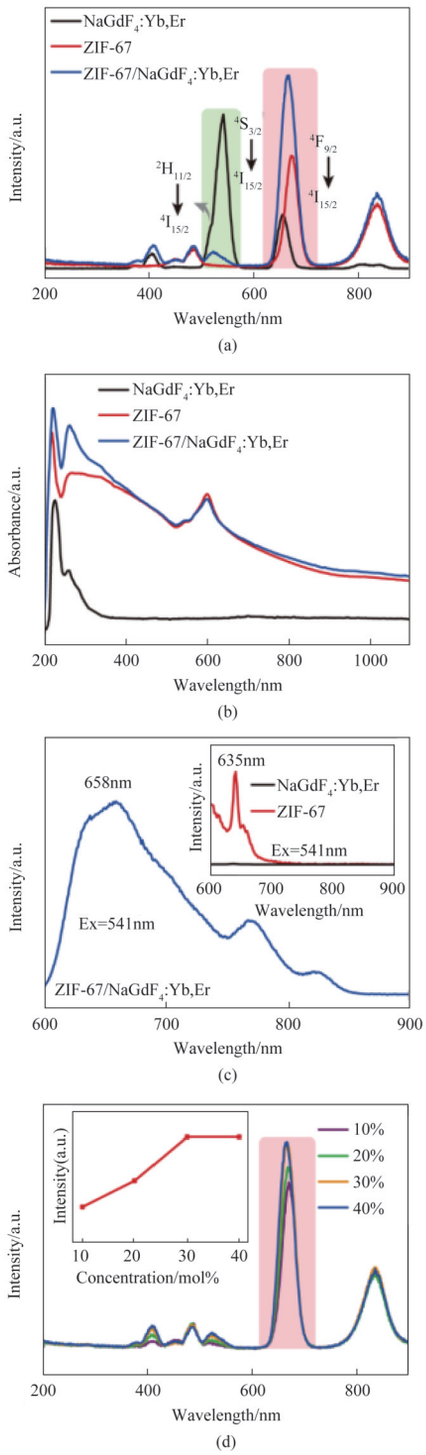

Fig. 4　Characterization and comparison of fluorescence properties of heterostructure ZIF-67/$NaGdF_4$: Yb, Er (a) UC PL spectra under 980 nm laser excitation, (b) UV-vis spectra, (c) PL emission spectra of heterostructure ZIF-67/$NaGdF_4$: Yb, Er, the inset is PL emission spectra of $NaGdF_4$: Yb, Er nanorods and ZIF-67, (d) UC PL spectra of heterostructure ZIF-67/$NaGdF_4$: Yb, Er with different concentration of $NaGdF_4$: Yb, Er nanorods, the inset is the variation of PL intensity

图4　异质结构ZIF-67/$NaGdF_4$: Yb, Er荧光性能的表征和对比(a)980 nm激发光下样品的上转换荧光性能,(b)样品的紫外吸收光谱,(c)样品的光致发光激发谱对比,(d)使用不同含量的$NaGdF_4$: Yb, Er纳米棒溶液制备得到的异质结构ZIF-67/$NaGdF_4$: Yb, Er的上转换荧光性能

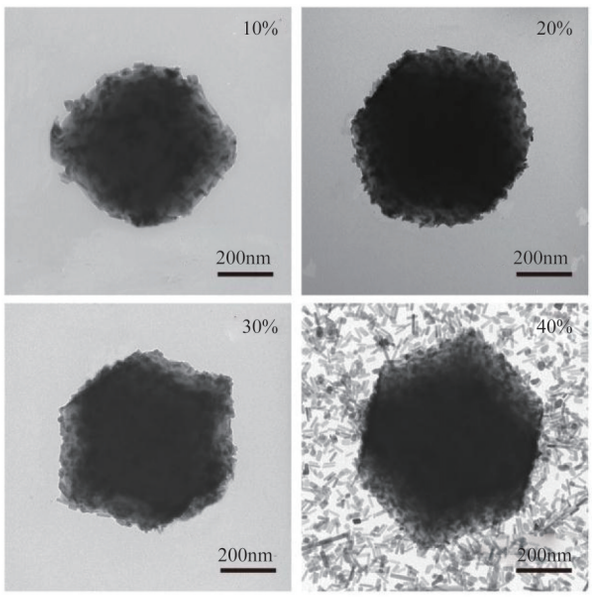

Fig. 5 TEM images of heterostructure ZIF-67/$NaGdF_4$: Yb, Er with different $NaGdF_4$: Yb, Er nanorods concentration
图5 使用不同含量 $NaGdF_4$: Yb, Er 纳米棒溶液制备得到的异质结构 ZIF-67/$NaGdF_4$: Yb, Er 的形貌

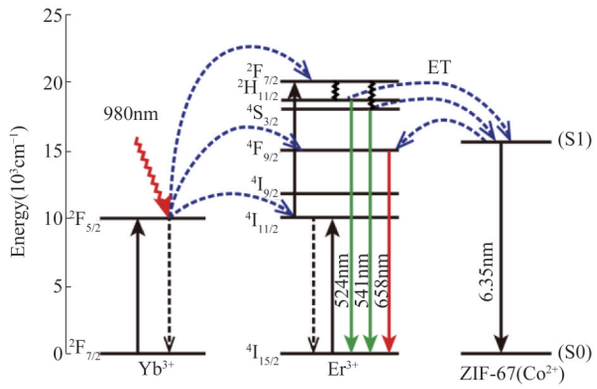

Fig. 6 Schematic energy level diagram showing the UC process mechanism of heterostructure ZIF-67/$NaGdF_4$: Yb, Er
图6 异质结构 ZIF-67/$NaGdF_4$: Yb, Er 中上转换机理的能级跃迁示意图

$^4I_{11/2}$ level of Er^{3+} causes the electrons in this level jumped to the $^4F_{7/2}$ state. And then the electrons relax rapidly to the $^2H_{11/2}$ and the $^4S_{3/2}$ states through multiphonon relaxation steps, leading to the green emission bands. The electrons in the $^4F_{9/2}$ level of Er^{3+} was following nonradiative transition process to the ground state $^4I_{15/2}$ of Er^{3+} by absorbing the additional excitation energy migrated from Yb^{3+} and producing the red emission [22-23]. The green light emitted at 524 nm and 541 nm, which were mainly derived from $^2H_{11/2}$ to $^4I_{15/2}$, $^4S_{3/2}$ to $^4I_{15/2}$ energy transfer, respectively [24]. And the red light emitted at 658 nm is mainly derived from $^4F_{9/2}$ to $^4I_{15/2}$ energy transfer. For heterostructure ZIF-67/$NaGdF_4$: Yb, Er, the new energy level is introduced from ZIF-67[20]. Just as the result revealed in Fig. 3(b) and 3(c), the energy at the $^2H_{11/2}$ and $^4S_{3/2}$ of Er^{3+} is transferred to S1 of Co^{2+} (form ZIF-67). And then energy at S1 of Co^{2+} transferred to $^4F_{9/2}$ of Er^{3+}, so that the PL intensity enhanced linearly. New energy transfer takes place in the heterostructure ZIF-67/$NaGdF_4$: Yb, Er, which is the key to the PL tuning and enhancement.

3 Conclusions

In summary, the heterostructure ZIF-67/$NaGdF_4$: Yb, Er was prepared by a facile stepwise synthesis method, the $NaGdF_4$: Yb, Er nanorods are uniformly loaded on the surface of ZIF-67. And the heterostructure overcame the shortcomings of $NaGdF_4$: Yb, Er nanorods in agglomeration and quench. Under the 980 nm laser excitation, the energy transfer takes place in the heterostructure ZIF-67/$NaGdF_4$: Yb, Er. And controllable PL tuning was realized by construction heterostructure the enhanced emission was converted from green light to red light. This strategy greatly enhances the applicability of heterostructure ZIF-67/$NaGdF_4$: Yb, Er, break through the limitation of oil phase system of $NaGdF_4$: Yb, Er nanorods, making it promising for biological imaging, bio-molecular detection and bio-sensor.

References

[1] Gudiksen M S, Lauhon L J, Wang J F, *et al*. Growth of nanowire superlattice structures for nanoscale photonics and electronics[J]. *Nature*, 2002, **415**:617-620.
[2] Mokari T, Sztrum C G, Salant A, *et al*. Formation of asymmetric one-sided metal-tipped semiconductor nanocrystal dots and rods[J]. *Nat. Mater*. 2005, **4**:855-863.
[3] Wang X T, Ouyang T, Wang L, *et al*. Redox-Inert Fe^{3+} Ions in Octahedral Sites of Co-Fe Spinel Oxides with Enhanced Oxygen Catalytic Activity for Rechargeable Zinc - Air Batteries[J]. *Angew. Chem. Int Edit*. 2019, **131**:13425-13430.
[4] LI Z, WANG C., CHEN X Z, *et al*. MoO_x nanoparticles anchored on N-doped porous carbon as Li-ion battery electrode[J]. *Chem. Eng*. J. 2020, 381.
[5] FAN S T, ZHANG J, TENG X L, *et al*. Self-Supported Amorphous SnO_2/TiO_2 Nanocomposite Films with Improved Electrochemical Performance for Lithium-Ion Batteries[J]. J. *Electrochem. Soc*. 2019, **166**: A3072-A3078.
[6] ZHENG F, SUN S J, FENG Y Q*et al*. Yb:$Ca_9Gd(VO_4)_7$, a potential ultrafast pulse laser crystal with promising spectral properties[J]. J. *Lumin*. 2020, **221**: 117085.
[7] JIAO J Q, BELFIORE L. A, SHEN W F.,et al. Fabrication and luminescence of $KGdF_4$: Yb^{3+}/Er^{3+} nanoplates and their improving performance for polymer solar cells[J]. *Sci. Bull*. 2019, **063**: 216-218.
[8] JIAO J Q, GAI S S., SHEN W F, *et al*. $NaYbF_4$: Tb/Eu modified with organic antenna for improving performance of polymer solar cells [J]. *Electrochim. Acta* 2018, **260**: 959-964.
[9] LI Y, JIAO J Q, YAN P, L. *et al*. Synthesis and tunable photoresponse for core-shell structured $NaGdF_4$: Yb, Er@SiO_2@Eu(TTA)$_3$Phen nanocomplexes[J]. *Scripta Mater*. 2018, **152**: 1-5.
[10] ZHANG Y Q, XU S, LI X P, *et al*. Improved LRET-based detection characters of Cu^{2+} using sandwich structured $NaYF_4$@ $NaYF_4$: Er^{3+}/Yb^{3+}@$NaYF_4$ nanoparticles as energy donor[J]. *Sensors Actuators B: Chemical* 2018, **257**: 829-838.
[11] LIU F Y, HE X X, LIU L, *et al*. Conjugation of $NaGdF_4$ upconverting nanoparticles on silica nanospheres as contrast agents for multi-modality imaging[J]. *Biomaterials* 2013, **34**: 5218-5225.
[12] XU Z H, Li C X, YANG P P. *et al*. Rare Earth Fluorides Nanowires/Nanorods Derived from Hydroxides: Hydrothermal Synthesis and Luminescence Properties[J]. *Cryst. Growth Des*. 2009, **9**: 4752-4758.
[13] LI Y T, TANG J L, HE L C, *et al*. Core-Shell Upconversion Nanoparticle@Metal-Organic Framework Nanoprobes for Luminescent/Magnetic Dual-Mode Targeted [J]. *Adv. Mater*. 2015, **27**: 4075-4080.
[14] Lv B Z, JIAO J Q, LIU Y, *et al*. Heterostructure $NaGdF_4$: Yb, Er an-

chored on MIL-101 for promoting photoelectronic response and photocatalytic activity[J]. *Nanoscale* 2019, **11**: 22730-22733.
[15] YAN C L, DADVAND A., ROSEI F., *et al*. Near-IR photoresponse in new up-converting CdSe/$NaYF_4$: Yb, Er nanoheterostructures[J]. J. *Am. Chem. Soci*. 2010, **132**: 8868-8869.
[16] Baumann A. E., Burns D. A., LIU B Q, *et al*. Metal-organic framework functionalization and design strategies for advanced electrochemical energy storage devices[J]. *Commun. Chem*. 2019, **2**: 86.
[17] HOSOYAMADA M., YAN A N., Okumura K., *et al*. Translating MOF chemistry into supramolecular chemistry: soluble coordination nanofibers showing efficient photon upconversion[J]. *Chem. Commun*. 2018, **54**: 6828-6831.
[18] LI M H, ZHENG Z J, ZHENG Y Q, *et al*. Controlled Growth of Metal-Organic Framework on Upconversion Nanocrystals for NIR-Enhanced Photocatalysis[J]. *ACS Appl. Mater. Inter*. 2017, **9**: 2899-2905.
[19] LI W Y, YANG F, Fang X J, *et al*. Systematic post-synthetic modification of metal-organic framework (ZIF-67) with superior cyclability for lithium-ion batteries[J]. *Electrochim. Acta* 2018, **282**: 276-285.
[20] ERGUSON J., WOOD D. L., UITERT L. G. V., Crystal-field spectra of d3, 7 ions. V. Tetrahedral CO^{2+} in $ZnAl_2O_4$ Spinel[J]. J. *Chem. Phys*. 1969, **51**: 2904-2910.
[21] DU P, LUO L H, YU J S, Controlled synthesis and upconversion luminescence of $Tm3^+$-doped $NaYbF_4$ nanoparticles for non-invasion optical thermometry[J]. *J. Alloy. Compd*. 2018, **739**: 926-933.
[22] TANG J, LI C, LI J, *et al*. Selectively enhanced red upconversion luminescence and phase/size manipulation via Fe^{3+} doping in $NaYF_4$: Yb, Er nanocrystals[J]. *Nanoscale* 2015, **7**: 14752-14759.
[23] ZHU Q, SONG C Y, LI X D, *et al*. Up-conversion monodispersed spheres of $NaYF_4$: Yb^{3+}/Er^{3+}: green and red emission tailoring mediated by heating temperature, and greatly enhanced luminescence by Mn^{2+} doping[J]. J. *Chem. Soc. Dalton* 2018, **47**: 8646-8655.
[24] TIAN Y Y, TIAN Y, HUANG P, *et al*. Effect of Yb^{3+} concentration on upconversion luminescence and temperature sensing behavior in Yb^{3+}/Er^{3+} co-doped YNbO4 nanoparticles prepared via molten salt route[J]. *Chem. Eng*. J. 2016, **297**: 26-34.